

Attachment of a Hydrogen-Bonding Carboxylate Side Chain to an [FeFe]-Hydrogenase Model Complex: Influence on the Catalytic Mechanism

Weiming Gao,^[a] Junliang Sun,^[b] Torbjörn Åkermark,^[c] Mingrun Li,^[b] Lars Eriksson,^[b] Licheng Sun,^[d] and Björn Åkermark*^[a]

Abstract: Azapropanedithiolate (adt)-bridged model complexes of [FeFe]-hydrogenase bearing a carboxylic acid functionality have been designed with the aim of decreasing the potential for reduction of protons to hydrogen. Protonation of the bisphosphine complexes **4–6** has been studied by in situ IR and NMR spectroscopy, which revealed that protonation with triflic acid most likely takes place first at the N-bridge for complex **4** but at the Fe–Fe bond

for complexes **5** and **6**. Using an excess of acid, the diprotonated species could also be observed, but none of the protonated species was sufficiently stable to be isolated in a pure state. Electrochemical studies have provided an insight into the catalytic mechanisms

Keywords: electrochemistry · electron transfer · enzyme model · iron-hydrogenase · proton reduction

under strongly acidic conditions, and have also shown that complexes **3** and **6** are electro-active in aqueous solution even in the absence of acid, presumably due to hydrogen bonding. Hydrogen evolution, driven by visible light, has been observed for three-component systems consisting of [Ru(bpy)₃]²⁺, complex **1**, **2**, or **3**, and ascorbic acid in CH₃CN/D₂O solution by on-line mass spectrometry.

Introduction

Efforts to determine the structure of the active site of [FeFe]-hydrogenases^[1] have led to extensive studies of models, such as azapropanedithiolate (adt) complexes of the type [Fe₂(CO)_{6-x}L_x{(SCH₂)₂NR}] (L = PMe₃). However,

even with these advanced structures, protons are reduced to hydrogen at a much more negative potential, usually < -1.5 V versus Fc/Fc⁺ (-1.12 V vs. SCE; -0.88 V vs. NHE) than with the natural hydrogenases (ca. -0.4 V vs. NHE; -1.02 V vs. Fc/Fc⁺ at pH 7).^[1] One explanation is that, unlike the hydrogenases, the synthetic models do not usually contain ligands such as cyanide; another could be that the ligand field of the natural protein surrounding is very different from those in the synthetic models.

During studies of synthetic models, it has often been found that protonation with strong acids is necessary to achieve hydrogen production even at potentials of about -1.5 V versus Fc/Fc⁺. The reason is that either protonation of the nitrogen of the adt bridge or the formation of iron hydrides, or indeed both, is required for proton reduction at a reasonable potential.^[2] In adt-bridged model complexes, on the other hand, the interaction between the NH proton and the FeH could aid in producing hydrogen at a reasonable potential.^[2] In nature, however, strong acids clearly cannot play an important role. It therefore occurred to us that in the natural hydrogenases nearby carboxyl groups could play a role, both through hydrogen bonding and by supplying protons, allowing the formation of hydrides under mild conditions. By participating in proton-coupled electron transfer (PCET) from the required electron donors, carboxyl groups should also be capable of lowering the redox potentials re-

[a] Dr. W. Gao, Prof. B. Åkermark
Department of Organic Chemistry, Arrhenius Laboratory
Stockholm University, 10691 Stockholm (Sweden)
Fax: (+46)8-154908
E-mail: bjorn.akermark@organ.su.se

[b] Dr. J. Sun, Dr. M. Li, Dr. L. Eriksson
Division of Structural Chemistry, Arrhenius Laboratory
Stockholm University, 10691 Stockholm (Sweden)

[c] Dr. T. Åkermark
Applied Electrochemistry
School of Chemical Science and Engineering
Royal Institute of Technology (KTH), 10044 Stockholm (Sweden)

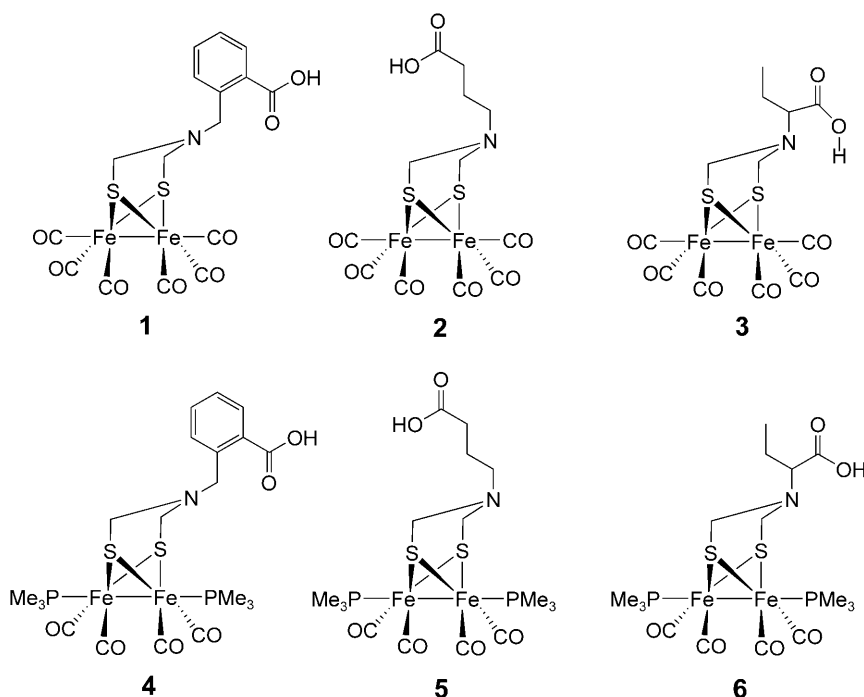
[d] Prof. L. Sun
Department of Chemistry
Royal Institute of Technology (KTH)
10044 Stockholm (Sweden)

Supporting information for this article is available on the WWW under <http://dx.doi.org/10.1002/chem.200902278>: Crystal structures of dimers of **1–3**; mechanisms A and B for CECE; cyclic voltammograms of **1–6** in the presence of incremental amounts of HOTf; and isotope distributions of evolved hydrogen with **2** and **3**.

quired for the generation of hydrogen.^[3] Although Darensbourg et al. and Talarmin et al. have reported a few Fe₂S₂ complexes bearing carboxylate groups that were shown to be efficient electrocatalysts in the presence of weak acids, strongly negative potentials were still required.^[4] We therefore decided to prepare some complexes of the type [Fe₂(CO)_{6-x}L_x{(SCH₂)₂NR}] (L = PMe₃) containing a carboxylate group capable of interacting with the adt nitrogen, and to study the redox potentials for proton reduction catalyzed by these complexes.

Results and Discussion

Preparation of complexes 1–6: The carboxylate-substituted diiron adt complexes **1–3** were synthesized according to Rauchfuss's route^[5] by reacting [Fe₂(CO)₆(HOCH₂S)₂] with the corresponding amino acids at -78 °C and then warming to room temperature. This gave the complexes **1–3** in moderate isolated yields (30–40%). Complexes **4–6** bearing two PMe₃ groups were then obtained in respective yields of around 50% by reacting complexes **1–3** with four equivalents of PMe₃ in refluxing THF. The ν(CO) bands in the IR



spectra of complexes **1–6**, along with those of previously reported propanedithiolate (pdt) complexes [Fe₂(CO)₆{μ-(SCH₂)₂CHCOOH}] (**7**) and [Fe₂(CO)₄(PMe₃)₂{μ-(SCH₂)₂CHCOOH}] (**8**), and adt complexes [Fe₂(CO)₄(PMe₃)₂{(μ-SCH₂)₂NCH₂C₆H₅}] (**9**) and [Fe₂(CO)₄(PMe₃)₂{(μ-SCH₂)₂NCH₂C₆H₄-2-Br}] (**10**), are summarized in Table 1.^[2a,4a,6a]

Table 1. IR data for complexes **1–6** as well as two pdt-diiron and two adt-diiron complexes for comparison.

Complex	ν(CO) _{Fe} [cm ⁻¹]	ν(C=O) _{OH} [cm ⁻¹]	Ref.
1	2073(m), 2029(s), 1991(s)	1691	[a]
2	2073(m), 2029(s), 1991(s)	1709	[a]
3	2074(m), 2033(s), 1994(s)	1710	[a]
4	1977(m), 1939(s), 1899(s)	1694	[a]
5	1979(m), 1938(s), 1896(s)	1665	[a]
6	1978(m), 1941(s), 1898(s)	1659	[a]
7 ^[b]	2077(m), 2034(s), 1992(s), 1978(sh)	1730	[4a]
8 ^[b]	1984(m), 1948(vs), 1903(s)	1729	[4a]
9 ^[c]	1981(m), 1943(vs), 1907(s), 1892(sh)	—	[2a]
10 ^[c]	1982(m), 1945(vs), 1901(s)	—	[6a]

[a] This work. [b] Spectrum recorded in THF. [c] Spectrum recorded in CH₃CN.

Properties of the complexes: When two of the six carbonyls were replaced by PMe₃ ligands, the average position of the three ν(CO)_{Fe} bands in the IR spectra shifted by about 90 cm⁻¹ to higher frequencies. The ³¹P NMR shifts of the complexes are similar, δ = 22.3 ppm for complexes **4** and **5** and δ = 22.7 ppm for **6**, and fall in the same range as the published shifts for related complexes.^[2a,4a,6a,b]

It is interesting to compare the IR frequencies of the carboxyl groups of the complexes. Among the hexacarbonyl complexes, a low carbonyl shift (1691 cm⁻¹), indicative of strong hydrogen bonding, was observed for the carboxyl group of complex **1**. This is presumably due to the formation of hydrogen-bonded dimers, as shown by the crystal structure determination. In contrast, the carbonyl frequencies for **2** and **3** are around 1710 cm⁻¹, indicating only weak hydrogen bonding, despite the fact that these complexes also form dimers in the crystalline state, with similar O–H...O distances (2.644 Å for **1**, 2.642 Å for **2**, and 2.669 Å for **3**; see the Supporting Information). This may possibly be because the carboxyl group is conjugated with the aromatic system in **1**.

The replacement of two carbonyl ligands by PMe₃ induced essentially no change on going from complex **1** to **4**, which seems to retain its dimeric structure, but for complexes **5** and **6** the low carbonyl frequencies of 1665 and 1659 cm⁻¹ indicate strong hydrogen bonding. A reasonable explanation is that the increased electron density on the diiron cluster that results from the presence of the phosphine donor ligands also renders the ni-

trogen sufficiently basic to participate in intramolecular hydrogen bonding to the carboxyl groups. This is shown by the fact that the IR frequency (1660 cm^{-1}) is unchanged when the spectrum of complex **6** is measured from a sample in THF, which should break intermolecular hydrogen bonds but not affect reasonably strong intramolecular bonds.^[7] In contrast, the IR frequency of the carboxyl groups in complex **8**, which lacks the nitrogen (1729 cm^{-1} in THF solution), shows that no intramolecular bond is formed in this complex.

It has previously been proposed that the protonated nitrogen of the adt bridge can participate by hydrogen bonding to an initially formed iron hydride and thereby serve to protonate the hydride to give molecular hydrogen.^[2b,e] Presumably, hydrogen bonding to the carboxylate can help to increase the mobility of the proton attached to the nitrogen. In addition, such hydrogen bonding could decrease the redox potential for the initial formation of iron hydride by facilitating proton-coupled electron transfer. This is illustrated for complex **6** in Scheme 1. First, proton-coupled reduc-

Molecular structures: The crystal structures of complexes **1–3** are shown in Figure 1, together with the atom-labeling system. Selected bond lengths and angles are given in Table 2.

Table 2. Selected metric data (bond lengths [Å] and angles [°]) for complexes **1–3**.

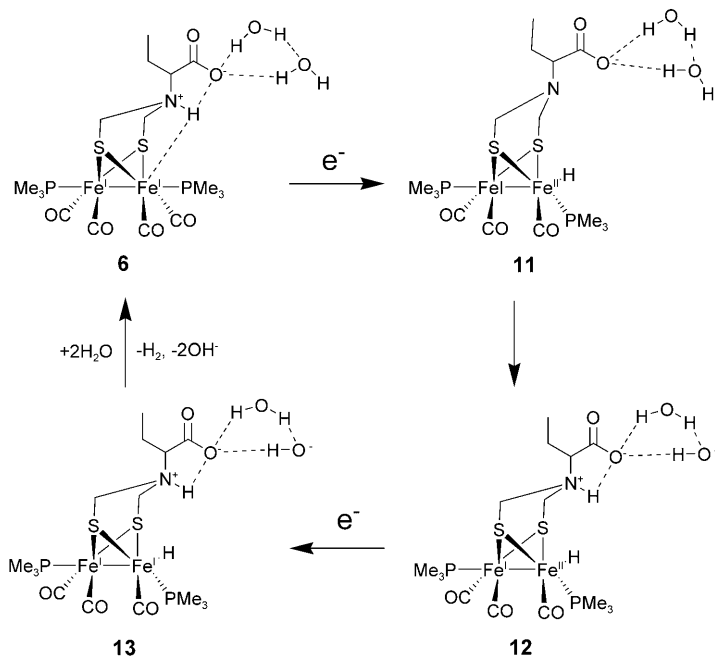
	1	2	3
Fe(1)-Fe(2)	2.506(2)	2.500(3)	2.5029(9)
Fe(1)-S(1)	2.255(3)	2.254(5)	2.2523(14)
Fe(1)-S(2)	2.250(3)	2.252(5)	2.2545(14)
Fe(1)-S(1)-Fe(2)	67.64(9)	67.53(13)	67.59(4)
S(1)-Fe(1)-S(2)	84.85(11)	85.03(16)	84.24(5)
C...N ^[a]	4.443	2.798	2.486
O(H)...N ^[b]	5.709	3.088	3.598

[a] The distance between the carbon (of the carboxylic acid) and the bridge nitrogen atom. [b] The nonbonding distance.

Each Fe_2S_2 subunit has a square-pyramidal structure. The Fe–Fe distances in complexes **1** (2.506 Å), **2** (2.500 Å), and **3** (2.503 Å) fall within the range commonly found for diiron model complexes.^[6,8,9] The structure of **1** is quite similar to that reported for the related complex $[\text{Fe}_2(\text{CO})_6\{(\mu\text{-SCH}_2)_2\text{NCH}_2\text{C}_6\text{H}_4\text{-2-Br}\}]$. The sum of the angles at the bridge N atom of **1** is 355° , which is very similar to that in $[\text{Fe}_2(\text{CO})_6\{(\mu\text{-SCH}_2)_2\text{NCH}_2\text{C}_6\text{H}_4\text{-2-Br}\}]$ (358°), suggesting near sp^2 -hybridization. The corresponding sum of the angles at N in **2** is similar (355°), while it is 340° in **3**, roughly consistent with sp^3 -hybridization at the nitrogen. This difference between **2** and **3** is surprising, since they both form carboxylic dimers in the solid state, with similar IR carbonyl frequencies (Table 1). However, in the solid state, the O–H...O bond is distinctly longer in **3** and the carboxyl group is oriented in such a way that it may also be involved in a hydrogen bond to the adt nitrogen, whereas the orientation in **2** makes this difficult.

Protonation of the complexes: We first studied the protonation of complexes **1–6** by a strong acid (HOTf, $\text{p}K_a = 2.60$). For complexes **1–3**, protonation was found to occur only at the adt nitrogen, even in the presence of five equivalents of HOTf, with a characteristic blue shift of the carbonyl frequencies ($\Delta\nu(\text{CO})_{\text{Fe}} \approx 17\text{ cm}^{-1}$). This is consistent with previously reported results concerning the protonation of adt complexes, such as $[\text{Fe}_2(\text{CO})_6\{(\mu\text{-SCH}_2)_2\text{NCH}_2\text{C}_6\text{H}_4\text{X}\}]$ (X = 2-Br, 4-Br) and $[\text{Fe}_2(\text{CO})_6\{(\mu\text{-SCH}_2)_2\text{NCH}_2\text{R}\}]$ (R = phenyl or alkyl).^[6]

For complex **6**, addition of one equivalent of HOTf resulted in a shift of the $\nu(\text{CO})_{\text{Fe}}$ bands to become a broad feature at about 2030 cm^{-1} . This large shift (ca. 50 cm^{-1}) is characteristic of protonation at the Fe–Fe bond (Figure 2b). On addition of five equivalents of HOTf, two well-defined $\nu(\text{CO})_{\text{Fe}}$ bands were seen at 2032 and 1993 cm^{-1} , clearly showing protonation of the Fe–Fe bond (Figure 2c). Upon further addition of HOTf up to 30 equivalents, these bands were shifted to 2046 and 2007 cm^{-1} . This additional shift, $\Delta\nu(\text{CO})_{\text{Fe}} = 14\text{ cm}^{-1}$, suggests formation of the hydride



Scheme 1.

tion of **6** yields the $\text{Fe}^{\text{I}}\text{Fe}^{\text{II}}$ hydride **11**. Reprotonation of the nitrogen then gives complex **12**, in which the interaction between the N-proton and the hydride makes the system predisposed for hydrogen evolution. In principle, this could occur directly, but it is more likely facilitated by a second electron transfer to give the $\text{Fe}^{\text{I}}\text{Fe}^{\text{I}}$ hydride **13**. Again, this electron transfer could be proton-coupled, facilitating the release of molecular hydrogen and giving **13** only as a short-lived intermediate. During or after these events, solvation of the formed hydroxide ions and their replacement by water regenerates the starting complex **6**.

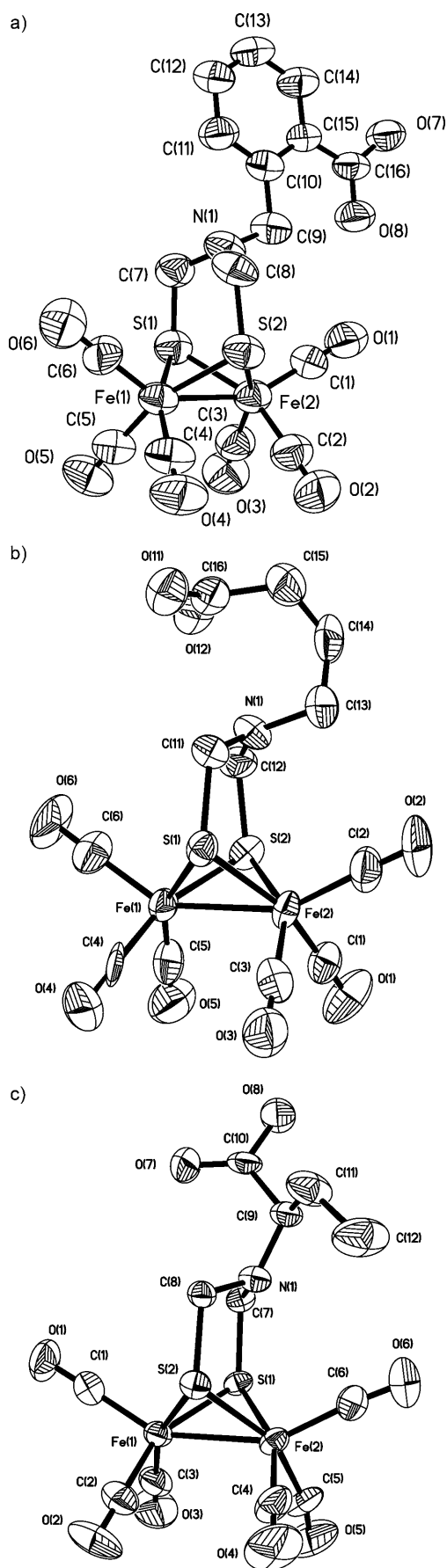


Figure 1. ORTEP diagrams (ellipsoids at 50% probability) of complexes **1** (a), **2** (b), and **3** (c).

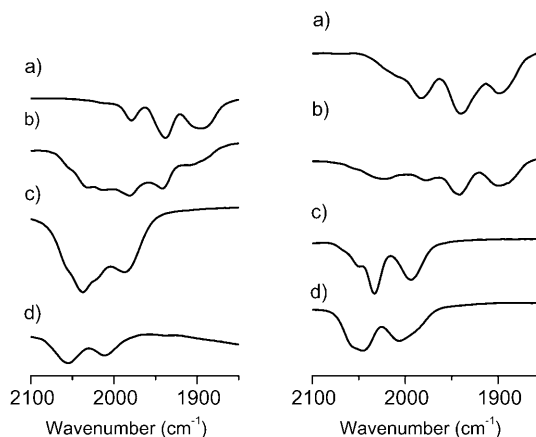


Figure 2. IR spectra of **5** (left) and **6** (right): a) in CH_3CN , b) + 1 equiv of HOTf, c) + 5 equiv of HOTf, d) + 30 equiv of HOTf.

$[\mathbf{6}(\text{NH})(\text{FeHFe})]^{2+}$ (Figure 2d). The frequencies, and the shifts thereof, for the two $\nu(\text{CO})_{\text{Fe}}$ bands are consistent with those reported for the diprotonated species of the related complexes $[\text{Fe}_2(\text{CO})_4(\text{PMe}_3)_2\{\mu\text{-SCH}_2\}_2\text{NCH}_2\text{C}_6\text{H}_5\}]$ (**9**) and $[\text{Fe}_2(\text{CO})_4(\text{PMe}_3)_2\{\mu\text{-SCH}_2\}_2\text{NCH}_2\text{C}_6\text{H}_4\text{-2-Br}\}]$ (**10**).^[6a,8] Upon addition of Et_3N , the $\nu(\text{CO})_{\text{Fe}}$ bands at 2046 and 2007 cm^{-1} reverted to 2032 and 1993 cm^{-1} , showing clean formation of the hydride $[\mathbf{6}(\text{FeHFe})]^+$.

Following the addition of 20 equivalents of HOTf to a solution of **6** in CD_3CN , the two protonated species $[\mathbf{6}(\text{FeHFe})]^+$ and $[\mathbf{6}(\text{NH})(\text{FeHFe})]^{2+}$ were present simultaneously according to in situ ^1H and ^{31}P NMR spectrometric analyses. The hydride triplet signal at $\delta = -15.59$ ppm (coupling constant $J_{\text{PH}} = 21.4$ Hz) is ascribed to $[\mathbf{6}(\text{FeHFe})]^+$, and the second hydride signal at $\delta = -15.57$ ppm (coupling constant $J_{\text{PH}} = 22.3$ Hz) is ascribed to $[\mathbf{6}(\text{NH})(\text{FeHFe})]^{2+}$. These values are very close to those reported previously for some related $\mu\text{-H}$ complexes.^[2a,6a] The ^{31}P NMR signals appeared at $\delta = 21.5$ ppm for $[\mathbf{6}(\text{FeHFe})]^+$ and at $\delta = 26.3$ and 22.3 ppm for $[\mathbf{6}(\text{NH})(\text{FeHFe})]^{2+}$ (Figure 3). The ^{31}P NMR spectra are thus consistent with the conclusions drawn from the IR spectra.

Complex **5** behaved in a similar way as complex **6** (Figure 3). The suggested protonation process is reasonable, since the $\text{p}K_{\text{a}}$ of the N-protonated species is around 10–12, while the $\text{p}K_{\text{a}}$ of the Fe hydride is around 15.^[2a,3a] For complex **4**, the protonation process was slightly different and similar to that described for complexes **9** and **10**.^[6a,8] As with these, the N-protonated species was the initial, metastable product, which spontaneously rearranged to the thermodynamically more stable Fe hydride species. This suggests that the carboxyl group does not influence the protonation of complex **4**. In contrast, the direct protonation of the Fe–Fe bond in **5** and **6** could be due to the fact that the nitrogen is engaged in hydrogen bonding to the carboxylate groups.

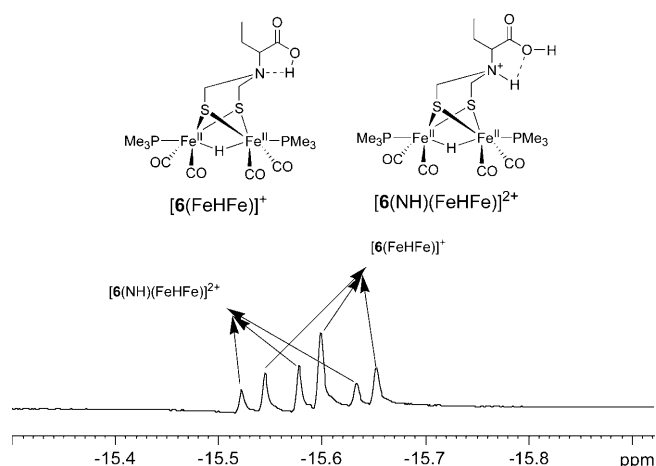


Figure 3. Hydride signals in a ^1H NMR spectrum attributable to $[\mathbf{6}(\text{FeHFe})]^+$ and $[\mathbf{6}(\text{NH})(\text{FeHFe})]^{2+}$ (obtained after treatment of complex **6** with 20 equivalents of HOTf).

Repeated attempts were made to obtain single crystals of $[\mathbf{6}(\text{FeHFe})]^+$ and $[\mathbf{6}(\text{NH})(\text{FeHFe})]^{2+}$. Unfortunately, these attempts failed, partly because the diprotonated species in particular was unstable in solution above 263 K. Solutions of the diprotonated forms of **6** and **5** spontaneously generated the μ -hydride complexes, for example $[\mathbf{6}(\text{FeHFe})]^+$, together with decomposition products, the structures of which have not been established.

Electrochemistry of complexes 1–3 under strongly acidic conditions (HOTf): Complexes **1–3** each displayed a reduction peak at about -1.6 V versus Fc/Fc^+ (Figure 4, Table 3).

Table 3. Electrochemical data of complexes **1–6** (V vs. Fc/Fc^+).

Complex	$E_{\text{pa}}^{\text{ox}} \text{Fe}^{\text{I}}\text{Fe}^{\text{I}}/\text{Fe}^{\text{II}}\text{Fe}^{\text{I}}$	$E_{\text{pc}} \text{Fe}^{\text{I}}\text{Fe}^{\text{I}}/\text{Fe}^{\text{0}}\text{Fe}^{\text{I}}$
1	+0.62	-1.61
2	+0.62	-1.60
3	+0.64	-1.63
4	-0.23	-2.01
5	-0.27	-2.05
6	-0.12	-1.94

On addition of one or two equivalents of triflic acid, their reduction peaks moved to about -1.20 V. This potential, about 400 mV more positive than the reduction potential of the starting materials, can be explained in terms of protonation of the nitrogen bridge.^[2] New reduction waves appeared at -1.54 V for **1** and **2**, and at -1.56 V for **3**. Upon the addition of more acid (3–10 equiv), the peak at -1.20 V was essentially unaffected, but for the new waves the currents grew linearly with increasing amount of acid. The peaks also shifted slightly to about -1.5 V. Similar results have recently been reported for the azadithiolate complex $[\text{Fe}_2(\text{CO})_6\{\mu\text{-SCH}_2\text{N}(\text{CH}_2\text{CH}_2\text{OMe})\text{CH}_2\text{S}\}]$.^[2b] For complex **2**, a third, sharp peak appeared at -1.36 V after addition of three equivalents of acid. This peak shifted with increasing acid concentration and after the addition of five equivalents it

had merged with the peak at about -1.5 V. Since this peak was only observed for complex **2**, it could perhaps be related to participation of the carboxyl group. Previously published structures of such N-protonated complexes with a nitrogen substituent suggest that upon protonation and subsequent sp^3 hybridization at the nitrogen, the proton will interact with the iron cluster and the substituent will occupy an axial position, pointing away from the cluster. However, a crude molecular model suggests that in the case of **2** the carbon chain is sufficiently long for interaction between the carboxyl group and the iron cluster even in this conformation. In principle, therefore, the peak could be the result of proton-coupled one-electron reduction of the complex, assisted by the carboxyl group.

Although the current increased only marginally with increasing acidity, on-line MS analysis of controlled-potential electrolysis at $E = -1.25$ V in a closed system in the presence of HOTf showed that complexes **1–3** catalyzed the formation of hydrogen at this potential. This suggests that both the initial monoprotonated complexes, such as $[(\text{Fe}^{\text{I}}\text{Fe}^{\text{I}})(\text{NH})]^+$, and the intermediate $[(\text{HFe}^{\text{II}}\text{Fe}^{\text{I}})(\text{NH})]^+$ are reduced at around -1.25 V. Similar results have recently been obtained by Talarmin, Gloaguen, and co-workers, using a complex with a methoxyethyl substituent on the nitrogen in place of the carboxylate groups presented here.^[3b] FTIR and CV analyses of the solid isolated from the solution after the electrolysis showed that the unchanged starting material could be recovered. The complexes **1–3** thus clearly act as catalysts and a CECE (chemical–electrochemical–chemical–electrochemical) mechanism (A) seems reasonable, in accordance with a recent proposal.^[3b] However, the observed redox potentials in the presence of strong acid also indicate the involvement of a second mechanism (B)^[3b] (see the Supporting Information).

Electrochemistry of complexes 4–6 under strongly acidic conditions (HOTf): Complexes **4–6**, in which two CO ligands have been replaced by PMe_3 , were also studied by CV in the presence of HOTf. Before the addition of acid, complexes **4** and **5** were reduced at potentials close to -2 V, while **6** was reduced at -1.9 V. Related complexes lacking the carboxyl group are generally reduced at potentials around -2.2 V.^[2a,8,10] It thus appears that the carboxyl groups contribute to lowering the potential for electron transfer, especially in complex **6**, in which the interaction should be strongest for steric reasons, in accordance with the relevant carboxyl IR frequencies (Table 1).

Upon addition of acid, the expected peak shifts were observed. For **4**, two reduction peaks were recorded, at -1.46 and -1.90 V. The shift of the peak at -1.46 V is of the same order (440 mV) as that observed upon protonation at nitrogen in related complexes such as $[\text{Fe}_2(\text{CO})_4(\text{PMe}_3)_2\{\mu\text{-SCH}_2\text{NCH}_2\text{C}_6\text{H}_4\text{-2-Br}\}]$.^[6a] Neither the magnitude nor the position of this peak changed significantly on increasing the acid concentration. The peak at -1.90 V also retained its position, but the current was directly proportional to the amount of added HOTf. This indicates that the N-protonat-

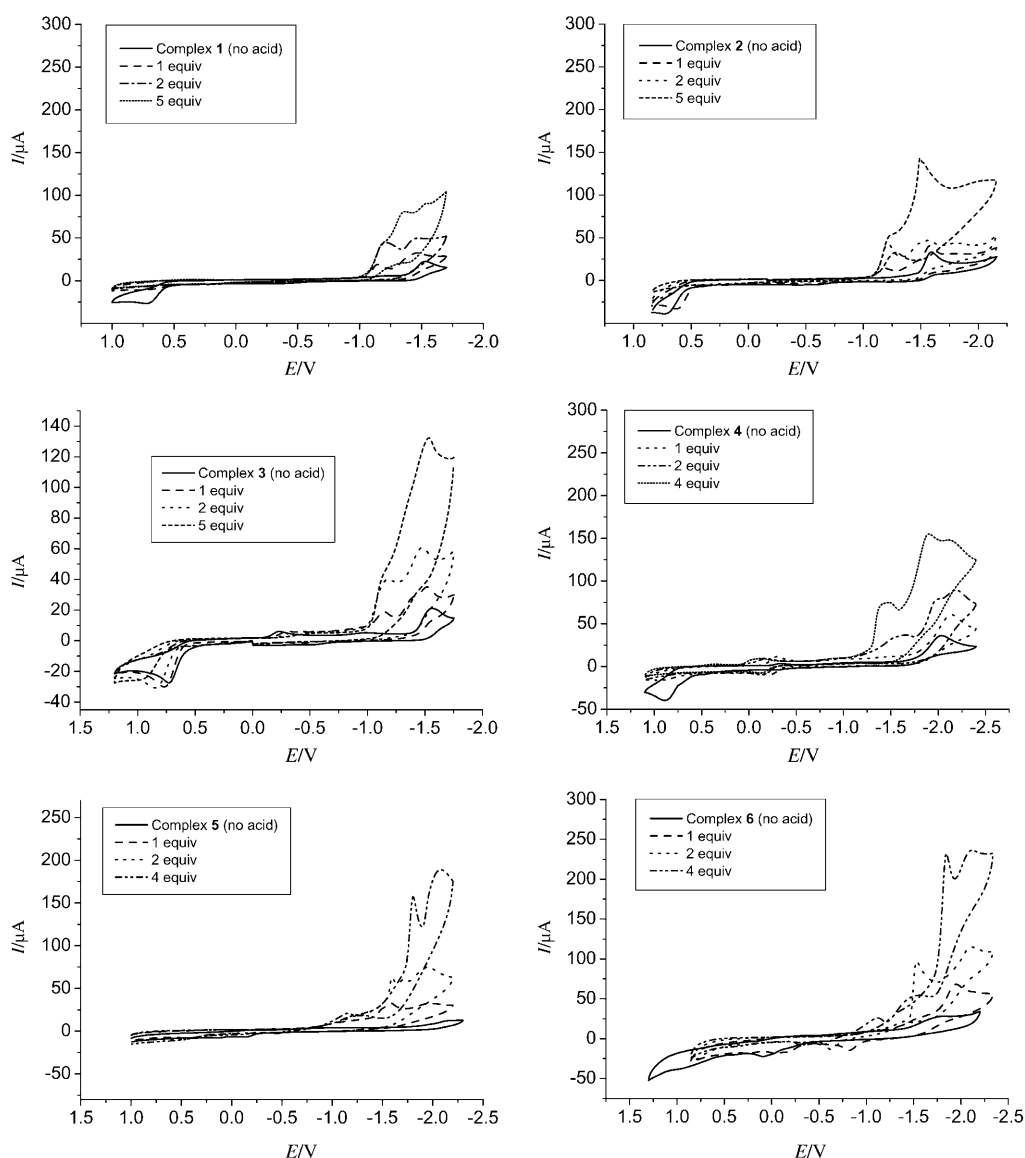


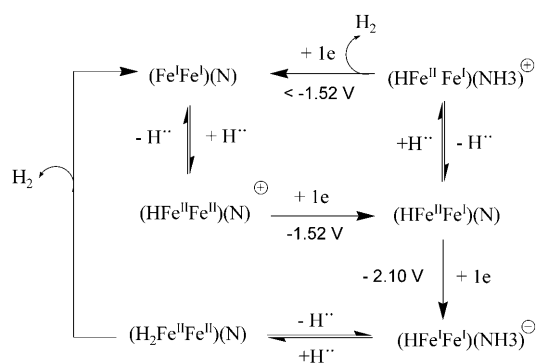
Figure 4. Cyclic voltammetry of complexes **1–6** (1 mM) in 0.05 M *n*Bu₄NPF₆/CH₃CN in the absence and presence of triflic acid at a scan rate of 100 mV s⁻¹.

ed species is electrochemically active in the reduction of protons. All of the reduction currents displayed a linear dependence of i_p on $v^{1/2}$, suggesting one-electron processes.

Complexes **5** and **6** behaved slightly differently. Only after addition of two equivalents of HOTf did new sharp peaks appear at -1.52 V for **6** (anodic shift 420 mV) and at -1.50 V for **5** (shift 550 mV). The intensities of these peaks increased only slightly on further addition of acid, but their potentials moved to more negative values, while at the same time a broad underlying reduction peak rapidly increased, starting at about -1 V. The increase of current vs amount of added acid was considerably greater for **5** and **6** (ca. 200 μ A after addition of 4 equiv of TfOH) than for **4** (ca. 50 μ A). For both **5** and **6**, curve crossing was observed after addition of about five equivalents of acid. The implication of this is not clear, but it suggests that a chemical reaction, such as re-

ductive elimination of hydrogen, gives an intermediate that is oxidized at the crossing potential, around -1.1 V. The electrochemical activity at each of the reduction peaks displayed a first-order dependence on [HOTf], and a one-electron reduction process was also indicated by the linear dependence of i_p on $v^{1/2}$. A simple CECE mechanism seems reasonable for the formation of hydrogen with these complexes (Scheme 2).

Light-driven hydrogen production: Light-driven hydrogen generation was studied in a similar way as previously reported, with a three-component system of [Ru(bpy)₃]²⁺, a diiron complex, and ascorbic acid (H₂A) in CH₃CN/D₂O solution.^[11] On-line MS was used to monitor the evolved gases in the molecular weight range 0–100. Hydrogen also appeared to be formed through processes other than the re-



Scheme 2.

duction of protons from water, for example from acetonitrile in the mass spectrometer. Deuterated water was therefore used in order to ensure that the hydrogen produced really derived from the added water.

The MS analysis of total evolved hydrogen (H_2 , HD, and D_2) as a function of reaction time for complexes **1–3** is shown in Figure 5. The initial slope of the hydrogen genera-

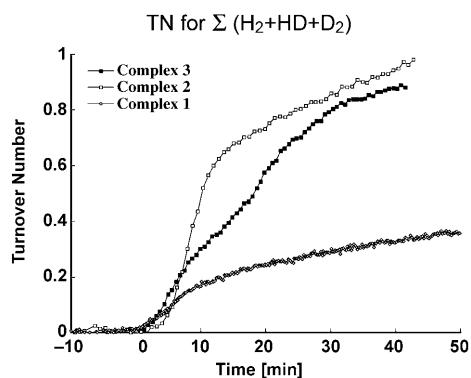


Figure 5. Evolved hydrogen studied by on-line gas analysis by recording mass spectra. ($[Ru(bpy)_3]^{2+}$, 1 μ mol; Fe_2S_2 , 5 μ mol; H_2A , 1 mmol; CH_3CN/D_2O , 2.5 mL:2.5 mL).

tion rate for complex **2** is about twice that for complex **3** and four times that for complex **1**. However, after about 40 min, almost the same amount of hydrogen had been formed by complexes **2** and **3**, close to three times that produced with **1**.

Analysis of hydrogen formation (H_2 , HD, and D_2) as a function of reaction time for complex **1** showed that the amount of hydrogen evolved first increased steadily and then leveled off after around 90 min at about 1 μ mol (Figure 6). The total amount of D_2 evolved was about twice that of HD and thrice that of H_2 . H_2 formation was essentially complete after 20 min, while the evolution of HD and D_2 continued for another 70 min. With complex **1**, the initial slopes for hydrogen evolution were about 23 $nmol\ min^{-1}$ for H_2 , 20 $nmol\ min^{-1}$ for HD, and 45 $nmol\ min^{-1}$ for D_2 .

Another important feature is that carbon monoxide was detected with a turnover number (TN) close to 3 after

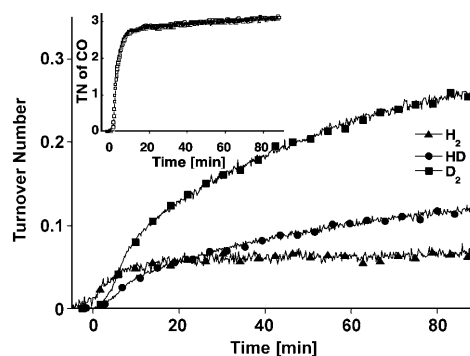


Figure 6. Isotope distribution of the evolved hydrogen, studied by on-line gas analysis by recording mass spectra. ($[Ru(bpy)_3]^{2+}$, 1 μ mol; complex **1**, 5 μ mol; H_2A , 1 mmol; CH_3CN/D_2O , 3.75 mL:1.25 mL).

20 min. This could explain the low TN number for hydrogen evolution, since it indicates photo-induced decomposition of the Fe_2S_2 complexes. Complexes **2** and **3** displayed similar photo-catalytic properties (Figure 6 and the Supporting Information).

Electrochemistry in aqueous solution: Finally, since Nature obviously cannot make use of strong acids, we were interested in ascertaining whether the carboxyl groups could influence the redox chemistry of the complexes **2**, **3**, **5**, and **6** in aqueous solution. With complex **2**, the effect appeared to be small, since the reduction peak at -1.6 V was essentially unaffected by addition of water to the solution in acetonitrile generally used. The second peak at around -2.2 V was also only marginally changed (Figure 7). The reduction potential of complex **3** at -1.6 V behaved in a similar way as that of complex **2**, although a small, steady increase in the current could be observed upon addition of increasing amounts of water. In contrast, at the second reduction of complex **3**, which was found at a less negative potential than in the case of **2** (-1.9 V), a sharp increase in the current was observed upon addition of 300 or 400 μ L of water. Although in the crystal structure **3** adopts a conformation in which the carboxyl group points away from the nitrogen, rotation to give a conformation with hydrogen bonding to the nitrogen could conceivably take place in a polar solvent, which would break the dimeric structure. Because the nitrogen here is not a strong hydrogen-bond acceptor, only a fairly small effect on redox behavior might be expected, in accordance with the experimental findings.

With complex **5**, a sharp increase in current was noted at about -2.3 V on addition of the first 50 μ L of water, but subsequent addition had little further effect. Complex **6** behaved differently, however. A small peak was observed at around -1.7 V, which increased slightly and moved to about -1.5 V with increasing addition of water. However, the most prominent effect was a sharp increase in current, starting at around -2 V, as more water was added. Decreases in the negative redox potentials for both **3** and **6** by about 300 mV to around -2 V, accompanied by sharp increases in the currents at these potentials, were observed (Figure 7).

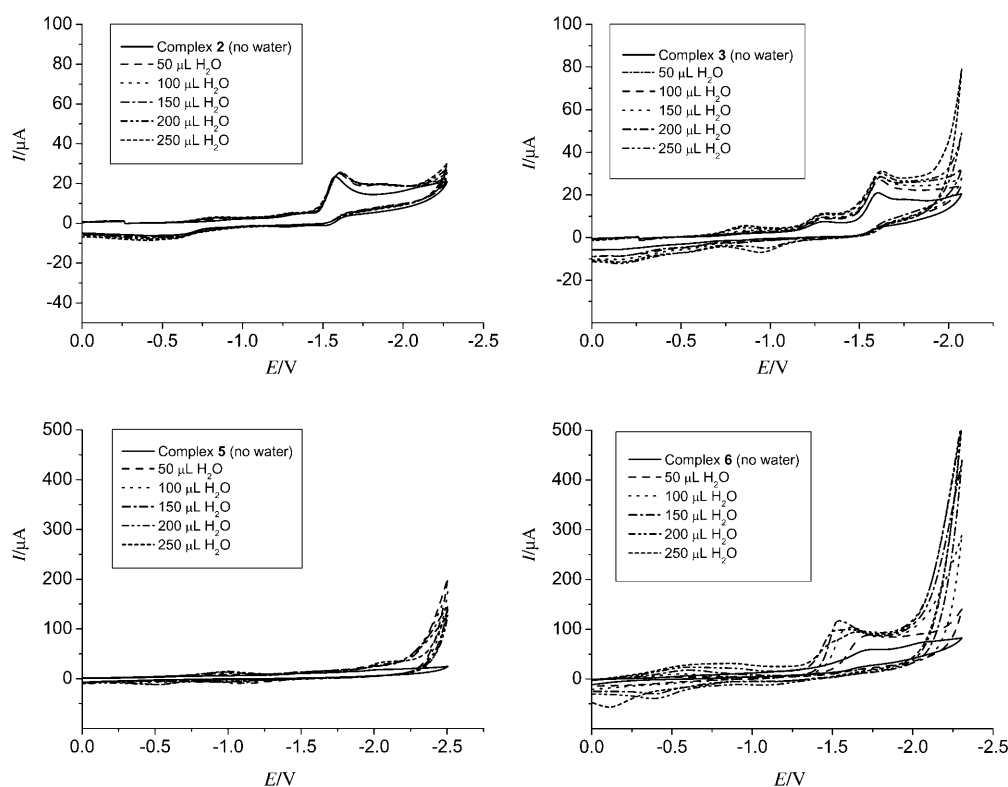


Figure 7. Cyclic voltammetry of complexes **2**, **3**, **5**, and **6** (1 mM) in 0.05 M *n*Bu₄NPF₆/CH₃CN in the presence of water at a scan rate of 100 mV s⁻¹.

These results are similar to those obtained by Lichtenberger and Darensbourg and their co-workers following the addition of acetic acid to Fe₂S₂ complexes.^[10] This shows that, at least in complex **6**, the carboxyl group does indeed play a role in the reduction of protons to molecular hydrogen.

Conclusion

In conclusion, a series of mimics of the active site of [FeFe]-hydrogenase, specifically adt-bridged Fe₂S₂ complexes **1–6** bearing carboxylic acid functionalities, has been prepared. Photoinduced hydrogen evolution is promoted by these complexes, and analysis by means of on-line MS showed the formation of D₂, HD, and H₂, although the turnover number was still low.

On treatment with triflic acid, complexes **1–3** are protonated exclusively at the nitrogen. In contrast, complexes **4–6**, in which two carbonyl ligands have been substituted by PMe₃ groups, undergo different protonation processes. In **4**, protonation occurs first on the bridging N, whereas the Fe–Fe bond is protonated first in **5** and **6**. Upon addition of strong acid, each of the complexes catalyzed the reduction of protons to hydrogen.

Interestingly, complexes **5** and **6** proved to be electrochemically active upon the addition of water alone, suggesting that the carboxyl group can promote proton reduction under neutral conditions. In natural hydrogenases, a number of neighboring amino acids are believed to participate

through proton transfer to the Fe₂S₂ site.^[1e,12,13] They might also be important for regulation of the potential for proton reduction, as suggested by the results for complexes **5** and **6**. Although this effect is small, it opens a fresh perspective in the construction of new types of hydrogenase models.

Experimental Section

General remarks: Unless otherwise indicated, all reactions and operations related to organometallic complexes were carried out under a dry, oxygen-free argon atmosphere using standard Schlenk techniques. Chemicals were purchased from Aldrich, and all solvents were dried and distilled prior to use according to the standard methods.

Infrared spectra were recorded on a Perkin–Elmer spectrum 1 spectrometer. NMR spectra were collected on a Varian spectrometer (400 MHz). Elemental analyses were performed at the Analytische Laboratorien, Lindar, Germany. Electro-spray mass spectrometry (FTICR-ESI-MS) was performed on a Bruker Daltonics BioAPEX-94e superconducting 9.4 Tesla FTICR mass spectrometer (Bruker Daltonics, Billerica, MA, USA).

Acetonitrile (Aldrich, spectroscopy grade) used in the electrochemistry experiments was dried with molecular sieves (4 Å) and then freshly distilled from CaH₂ under an argon atmosphere. A solution of 0.05 M *n*Bu₄NPF₆ (Fluka, electrochemical grade) in CH₃CN was used as electrolyte. Electrochemical measurements were carried out in a three-electrode cell connected to an Autolab potentiostat with a GPES electrochemical interface. The working electrode was a glassy carbon disc (diameter 2 mm, freshly polished). The reference electrode was a non-aqueous Ag/Ag⁺ electrode (1.0 mm AgNO₃ in CH₃CN) with the ferrocene/ferrocenium (Fc/Fc⁺) couple as an external standard. The auxiliary electrode was a platinum wire. All potentials reported herein are quoted relative to the

Fe/Fc⁺ couple. The solutions were purged with solvent-saturated argon to remove residual oxygen. All experimental measurements were made while maintaining the systems under an atmosphere of argon at all times. Single-crystal X-ray diffraction patterns were recorded with an Oxford Diffraction Excalibur diffractometer equipped with a sapphire-3 CCD using an Mo_{Kα} radiation source ($\lambda = 0.71073 \text{ \AA}$) with ω scans at different ϕ values to fill the Ewald sphere. The sample-to-detector distance was 50 mm. The maximum value of 2θ was 63° .

Indexing, cell refinements, and integration of reflection intensities were performed with Crystalis software.^[14] Numerical absorption correction was performed with the program X-RED,^[15] verifying the crystal shape with the program X-shape.^[16] The structure was solved by direct methods using SHELXS-97,^[17] which yielded electron density maps in which most of the non-hydrogen atoms could be resolved. The rest of the non-hydrogen atoms were located from difference electron density maps, and the structure model was refined through full-matrix least-squares calculations on F^2 using the program SHELXL97-2.^[18] All non-hydrogen atoms were refined with anisotropic displacement parameters, while the hydrogens, which were placed in geometrically calculated positions and allowed to ride on the atoms to which they were bonded, were given isotropic displacement parameters calculated as $\xi(U_{eq})$ for the non-hydrogen atoms), with $\xi = 1.2$ for methylenic ($-\text{CH}_2-$) and aromatic hydrogens.

CCDC-744052 (**1**), CCDC-744053 (**2**), and CCDC-744054 (**3**) contain the supplementary crystallographic data for this paper. These data can be obtained free of charge from The Cambridge Crystallographic Data Centre via www.ccdc.cam.ac.uk/data_request/cif.

Gas analysis by mass spectrometry: The mass spectrometer set-up used consisted of three separate parts connected with gas valves^[19–23] (see Figure 8), namely an enclosed volume (or reaction chamber), a gas han-

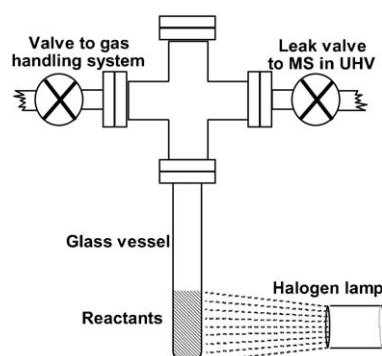


Figure 8. The experimental set-up for gas analysis by recording mass spectra.

dling system (GHS), and a mass spectrometer (MKS Spectra Products, Microvision Plus, 0–100 mass units) under ultra-high vacuum (base pressure 2×10^{-10} bar). The GHS permitted control of the atmosphere in the enclosed volume. Almost any gas reservoir could be connected to the GHS and, in principle, the only limitation was that the vapor pressure of the gases used had to be higher than 1 mbar. A rough pump was used to evacuate the GHS, so that the pressure could be regulated in the range 0.1–1000 mbar. With this set-up, the enclosed volume was continuously probed by the mass spectrometer through an inlet regulated by a leak valve. The inlet to the mass spectrometer was so small that the probing caused a negligible pressure change in the enclosed volume. Consequently, the measurements had a negligible influence on the measured reaction rates. The measured data comprised partial pressures in the MS of masses 0–100 versus time. By calibration of the system, these measured data could be converted into partial pressures of the different components in the enclosed volume. As the volume and temperature of the enclosed volume were known, by applying the gas laws the partial pressures of the different components could be converted into the amounts of

these components in the enclosed volume. This permitted a quantitative determination of the amounts of gases produced with masses in the interval 1–100 mass units.

In studies of photochemical hydrogen generation, a glass tube was attached to the enclosed volume (Figure 8). Deuterated water/acetonitrile (5 mL), $[\text{Ru}(\text{bpy})_3(\text{PF}_6)_2]$ (1 μmol), H_2A (1 mmol), and complex **1**, **2**, or **3** (5 μmol) were mixed in a test tube. The total volume of water and acetonitrile was kept at 5 mL, but with ratios of water to acetonitrile of 1:30, 1:3, 1:1, and 3:1. The test tube was then attached to the enclosed volume, which was evacuated for ~ 5 min to minimize the amount of dissolved gases in the solution. Ar at ~ 30 mbar was then introduced into the enclosed volume. The inlet to the MS was adjusted, and after a period of at least 10 min, during which the partial pressures in the MS stabilized, the light was switched on. In this way, the start of the experiment was well defined. The light source used was a 150 W halogen lamp. As the reactions were conducted in a glass vessel, the mixtures could be illuminated directly through the glass walls of the reactor. In some experiments, a Pyrex glass UV filter was used, but this had negligible effect on the reactions.

$\text{H}_2\text{NCH}_2\text{C}_6\text{H}_4\text{-2-COOH-HCl}$: The starting compound phthalimidine (1.33 g, 10 mmol), prepared according to a literature procedure,^[24] was refluxed in 37% HCl (140 mL) for 10 h. Removing the solvent under reduced pressure and washing the residue with CHCl_3 (20 mL) afforded the target (2-benzylamino)carboxylic acid (HCl salt) as a white solid (1.31 g, 70%). $^1\text{H NMR}$ (D_2O): $\delta = 4.27$ (s, 2H; CH_2), 7.35–7.50 (m, 2H; C_6H_4), 7.57 (t, $J = 7.4$ Hz, 1H; C_6H_4), 7.97 ppm (d, $J = 7.6$ Hz, 1H; C_6H_4); MS (ESI-TOF): m/z : 152.072 $[\text{M}+\text{H}]^+$.

$[\text{Fe}_2(\text{CO})_6(\mu\text{-SCH}_2)_2\text{NCH}_2\text{C}_6\text{H}_4\text{-2-COOH}]$ (1**):** A solution of (2-benzylamino)carboxylic acid (HCl salt) (0.25 g, 1.3 mmol) and Et_3N (0.18 mL, 1.3 mmol) in THF (40 mL) was stirred for 0.5 h at room temperature and then cooled to 0°C . A solution of $[\text{Fe}_2(\text{CO})_6(\text{HOCH}_2\text{S})_2]$ ^[5] (1.28 mmol) in THF (20 mL) was then added. After allowing the reaction to proceed for 5 h, the solution was filtered and the solvent was removed on a rotary evaporator. The crude product was purified by column chromatography with $\text{CH}_2\text{Cl}_2/\text{CH}_3\text{COCH}_3$ (10:1, v/v) as eluent to give **1** (200 mg, 30%) as a red solid. $^1\text{H NMR}$ (CDCl_3): $\delta = 3.68$ (s, 4H; $2 \times \text{NCH}_2\text{S}$), 4.35 (s, 2H; $\text{C}_6\text{H}_4\text{CH}_2\text{N}$), 7.32 (d, $J = 7.5$ Hz, 1H; C_6H_4), 7.42 (t, $J = 7.5$ Hz, 1H; C_6H_4), 7.57 (t, $J = 7.4$ Hz, 1H; C_6H_4), 8.11 ppm (d, $J = 7.6$ Hz, 1H; C_6H_4); IR (CH_2Cl_2): $\nu(\text{CO}) = 2073, 2029, 1991, 1691 \text{ cm}^{-1}$; elemental analysis calcd (%) for $\text{C}_{16}\text{H}_{11}\text{Fe}_2\text{NO}_8\text{S}_2$: C 36.88, H 2.13, N 2.69; found: C 37.04, H 2.43, N 2.95.

$[\text{Fe}_2(\text{CO})_6(\mu\text{-SCH}_2)_2\text{NCH}_2\text{CH}_2\text{CH}_2\text{COOH}]$ (2**):** 4-Aminobutyric acid (0.515 g, 5 mmol) was added directly to a solution of $[\text{Fe}_2(\text{CO})_6(\text{HOCH}_2\text{S})_2]$ (2 mmol) in THF (40 mL) at -78°C . After warming to room temperature, the solution was filtered and then the solvent was removed on a rotary evaporator. The crude product was purified by column chromatography with $\text{CH}_2\text{Cl}_2/\text{CH}_3\text{COCH}_3$ (10:1, v/v) as eluent to give **2** (389 mg, 41%) as a red solid. $^1\text{H NMR}$ (CD_3CN): $\delta = 1.70$ (s, 2H; $\text{CH}_2\text{CH}_2\text{CH}_2$), 2.39 (m; CH_2COOH), 2.79 (s, 2H; $\text{CH}_2\text{CH}_2\text{N}$), 3.56 ppm (s, 4H; NCH_2S); IR (CH_2Cl_2): $\nu(\text{CO}) = 2073, 2029, 1991, 1734 \text{ cm}^{-1}$; elemental analysis calcd (%) for $\text{C}_{10}\text{H}_{11}\text{Fe}_2\text{NO}_8\text{S}_2$: C 30.47, H 2.34, N 2.96; found: C 30.81, H 2.75, N 3.14.

$[\text{Fe}_2(\text{CO})_6(\mu\text{-SCH}_2)_2\text{NCH}(\text{CH}_2\text{CH}_3)\text{COOH}]$ (3**):** 2-Aminobutyric acid (0.515 g, 5 mmol) was added directly to a solution of $[\text{Fe}_2(\text{CO})_6(\text{HOCH}_2\text{S})_2]$ (2 mmol) in THF (40 mL) at -78°C . After warming to room temperature, the solution was filtered and then the solvent was removed on a rotary evaporator. The crude product was purified by column chromatography with $\text{CH}_2\text{Cl}_2/\text{CH}_3\text{COCH}_3$ (10:1, v/v) as eluent to give **3** (389 mg, 41%) as a red solid. $^1\text{H NMR}$ (CD_3CN): $\delta = 0.85$ (t, $J = 7.5$ Hz, 3H; CH_3), 1.71 (m, 2H; $\text{CH}_2\text{CH}_2\text{CH}$), 3.16 (t, $J = 7.3$ Hz, 1H; $\text{CH}_2\text{CHNCOOH}$), 3.37 (d, $J = 12.0$ Hz, 2H; NCH_2S), 3.47 ppm (d, $J = 12.0$ Hz, 2H; NCH_2S); IR (CH_2Cl_2): $\nu(\text{CO}) = 2074, 2033, 1994, 1710 \text{ cm}^{-1}$; elemental analysis calcd (%) for $\text{C}_{12}\text{H}_{11}\text{Fe}_2\text{NO}_8\text{S}_2$: C 30.47, H 2.34, N 2.96; found: C 30.91, H 2.69, N 3.15.

$[\text{Fe}_2(\text{CO})_6(\text{PMe}_3)_2(\mu\text{-SCH}_2)_2\text{NCH}_2\text{C}_6\text{H}_4\text{-2-COOH}]$ (4**):** A solution of **1** (0.052 g, 0.1 mmol) and PMe_3 (0.4 mL, 0.4 mmol, 1 M in THF) in THF (20 mL) was refluxed for 3.5 h. The solvent was then removed and the crude product was purified by column chromatography with $\text{CH}_3\text{COCH}_3/$

CH₃OH/Et₃N (200:10:1, v/v/v) as eluent to give **4** (32 mg, 51%). ¹H NMR (CD₃CN): δ = 1.50 (d, *J* = 9.2 Hz, 18H; PCH₃), 3.21 (s, 4H; 2 × NCH₂S), 4.09 (s, 2H; C₆H₄CH₂N), 7.28 (s, 3H; C₆H₄), 7.63 ppm (s, 1H; C₆H₄); ³¹P NMR (CD₃CN): δ = 22.33 ppm; IR (CH₂Cl₂): ν(CO) = 1977, 1939, 1899, 1694 cm⁻¹; elemental analysis calcd (%) for C₂₀H₃₁NFe₂O₆P₂S₂: C 38.79, H 5.05, N 2.26; found: C 39.25, H 5.51, N 1.79.

[Fe₂(CO)₄(PMe₃)₂(μ-SCH₂)₂NCH₂CH₂CH₂COOH] (5): A solution of **2** (0.047 g, 0.1 mmol) and PMe₃ (0.4 mL, 0.4 mmol, 1 M in THF) in THF (20 mL) was refluxed for 3.5 h. The solvent was then removed and the crude product was purified by column chromatography with CH₃COCH₃/CH₃OH/Et₃N (200:10:1, v/v/v) as eluent to give **5** (29 mg, 51%). ¹H NMR (CD₃CN): δ = 1.53 (d, *J* = 9.3 Hz, 18H; PCH₃), 1.97 (m, 2H; CH₂CH₂CH₂), 2.36 (s, 2H; CH₂COOH), 2.51 (s, 2H; CH₂CH₂N), 3.23 ppm (s, 4H; 2 × NCH₂S); ³¹P NMR (CD₃CN): δ = 22.36 ppm; IR (CH₂Cl₂): ν(CO) = 1979, 1938, 1896, 1665 cm⁻¹; elemental analysis calcd (%) for C₁₆H₂₀Fe₂NO₆P₂S₂: C 33.76, H 5.14, N 2.46; found: C 34.05, H 5.53, N 2.49.

[Fe₂(CO)₄(PMe₃)₂(μ-SCH₂)₂NCH(CH₂CH₃)COOH] (6): A solution of **3** (0.047 g, 0.1 mmol) and PMe₃ (0.4 mL, 0.4 mmol, 1 M in THF) in THF (20 mL) was refluxed for 3.5 h. The solvent was then removed and the crude product was purified by column chromatography with CH₃COCH₃/CH₃OH/Et₃N (200:10:1, v/v/v) as eluent to give **6** (28 mg, 50%). ¹H NMR (CD₃CN): δ = 1.32 (t, *J* = 4.5 Hz, 3H; CH₂CH₃), 1.50 (s, 18H; PCH₃), 1.55 (m, 2H; CHCH₂CH₃), 3.41 (s, 1H; CH₂CHNCOOH), 3.58 ppm (s, 4H; 2 × NCH₂S); ³¹P NMR (CD₃CN): δ = 22.7 ppm; IR (CH₂Cl₂): ν(CO) = 1978, 1941, 1898, 1659 cm⁻¹; elemental analysis calcd (%) for C₁₆H₂₀Fe₂NO₆P₂S₂: C 33.76, H 5.14, N 2.46; found: C 34.05, H 5.53, N 2.49.

Protonation of complex 6: Complex **6** (5.7 mg, 0.01 mmol) was dissolved in CD₃CN (0.5 mL) in an NMR tube under argon atmosphere to give a red solution. Incremental amounts of triflic acid (1 equiv: 0.88 μL) were then added directly to the solution for in situ ¹H NMR, ³¹P NMR, and IR analyses. All attempts to isolate the protonated complexes were unsuccessful.

Acknowledgements

We are grateful to the Swedish Research Council, the K&A Wallenberg Foundation, and the Swedish Energy Agency for financial support of this work.

- [1] a) A. L. De Lacey, V. M. Fernández, M. Rousset, R. Cammack, *Chem. Rev.* **2007**, *107*, 4304–4330; b) P. M. Vignais, B. Billoud, *Chem. Rev.* **2007**, *107*, 4206–4272; c) G. J. Kubas, *Chem. Rev.* **2007**, *107*, 4152–4205; d) W. Lubitz, E. Rejers, M. Van Gastel, *Chem. Rev.* **2007**, *107*, 4331–4365; e) J. C. Fontecilla-Camps, A. Volbeda, C. Cavazza, Y. Nicolet, *Chem. Rev.* **2007**, *107*, 4273–4303; f) F. Gloaguen, T. B. Rauchfuss, *Chem. Soc. Rev.* **2009**, *38*, 100–108; g) C. Tard, C. J. Pickett, *Chem. Rev.* **2009**, *109*, 2245–2274.
- [2] a) G. Eilers, L. Schwartz, M. Stein, G. Zampella, L. De Gioia, S. Ott, R. Lomoth, *Chem. Eur. J.* **2008**, *14*, 7075–7084; b) J.-F. Capon, S. Ezzaher, F. Gloaguen, F. Y. Pétilion, P. Schollhammer, J. Talarmin, *Chem. Eur. J.* **2008**, *14*, 1954–1964; c) B. E. Barton, M. T. Olsen, T. B. Rauchfuss, *J. Am. Chem. Soc.* **2008**, *130*, 16834–16835.
- [3] a) M. H. V. Huynh, T. J. Meyer, *Chem. Rev.* **2007**, *107*, 5004–5064; b) C. Costentin, *Chem. Rev.* **2008**, *108*, 2145–2179.
- [4] a) C. M. Thomas, O. Rüdiger, T. Liu, C. E. Carson, M. B. Hall, M. Y. Darensbourg, *Organometallics* **2007**, *26*, 3976–3984; b) V. Vijai-kanth, J. F. Capon, F. Gloaguen, F. Y. Pétilion, P. Schollhammer, J. Talarmin, *J. Organomet. Chem.* **2007**, *692*, 4177–4181.
- [5] a) H. Li, T. B. Rauchfuss, *J. Am. Chem. Soc.* **2002**, *124*, 726–727; b) J. L. Stanley, Z. M. Heiden, T. B. Rauchfuss, S. R. Wilson, L. De Gioia, G. Zampella, *Organometallics* **2008**, *27*, 119–125.
- [6] a) F. Wang, M. Wang, X. Liu, K. Jin, W. Dong, L. Sun, *Dalton Trans.* **2007**, 3812–3819; b) S. Ott, M. Kritikos, B. Åkermark, L. Sun, R. Lomoth, *Angew. Chem.* **2004**, *116*, 1024–1027; *Angew. Chem. Int. Ed.* **2004**, *43*, 1006–1009; c) W. Gao, J. Liu, C. Ma, L. Weng, K. Jin, C. Chen, B. Åkermark, L. Sun, *Inorg. Chim. Acta* **2006**, *359*, 1071–1080; d) W. Gao, J. Ekström, J. Liu, C. Chen, L. Eriksson, L. Weng, B. Åkermark, L. Sun, *Inorg. Chem.* **2007**, *46*, 1981–1991.
- [7] B. Åkermark, *Acta Chem. Scand.* **1961**, *15*, 985–990.
- [8] L. Schwartz, G. Eilers, L. Eriksson, A. Gogoll, R. Lomoth, S. Ott, *Chem. Commun.* **2006**, 520–522.
- [9] a) W. Gao, J. Liu, B. Åkermark, L. Sun, *Inorg. Chem.* **2006**, *45*, 9169–9171; b) L. Song, J. Ge, X. Liu, L. Zhao, Q. Hu, *J. Organomet. Chem.* **2006**, *691*, 5701–5709; c) L. Song, H. Wang, J. Ge, S. Mei, J. Gao, L. Wang, B. Gai, L. Zhao, J. Yan, Y. Wang, *Organometallics* **2008**, *27*, 1409–1416; d) K. Justice, G. Zampella, L. De Gioia, T. B. Rauchfuss, J. I. Van der Vlugt, S. R. Wilson, *Inorg. Chem.* **2007**, *46*, 1655–1664.
- [10] a) D. Chong, I. P. Georgakaki, R. Meija-Rodriguez, J. Sannabria, M. P. Soriaga, M. Y. Darensbourg, *Dalton Trans.* **2003**, 4158–4163; b) G. A. N. Felton, A. K. Vanucci, J. Chen, L. T. Lockett, N. Okumura, B. J. Petro, U. I. Zakai, D. H. Evans, R. S. Glass, D. L. Lichtenberger, *J. Am. Chem. Soc.* **2007**, *129*, 12521–12530.
- [11] a) Y. Na, M. Wang, J. Pan, P. Zhang, B. Åkermark, L. Sun, *Inorg. Chem.* **2008**, *47*, 2805–2810; b) X. Li, M. Wang, S. Zhang, J. Pan, Y. Na, J. Liu, B. Åkermark, L. Sun, *J. Phys. Chem. B* **2008**, *112*, 8198–8202.
- [12] Y. Nicolet, C. Piras, P. Legrand, C. E. Hatchikian, J. C. Fontecilla-Camps, *Structure* **1999**, *7*, 13–23.
- [13] J. W. Peters, W. N. Lanzilotta, B. J. Lemon, L. C. Seefeldt, *Science* **1998**, *282*, 1853–1858.
- [14] Xcalibur CCD system, CrysAlis Software system, Version 1.170, Oxford Diffraction Ltd., Oxford, **2003**.
- [15] X-RED, absorption correction program, Version 1.09, Stoe & Cie GmbH Darmstadt, Darmstadt.
- [16] X-SHAPE, Crystal Optimisation for Numerical Absorption Correction, Version 1.2, Stoe & Cie GmbH Darmstadt, Darmstadt.
- [17] G. M. Sheldrick, *Acta Crystallogr. Sect. A* **1990**, *46*, 467.
- [18] SHELXL97–2, Computer program for the refinement of crystal structures, G. M. Sheldrick, University of Göttingen, Göttingen, **1997**.
- [19] G. Hultquist, L. Gräsjö, Q. Lu, T. Åkermark, *Corr. Sci.* **1994**, *36*, 1459–1471.
- [20] T. Åkermark, J.-J. Ganem, I. Trimaille, S. Rigo, *J. Electrochem. Soc.* **1999**, *146*, 4580–4585.
- [21] T. Åkermark, B. Emmoth, H. Bergsäker, *J. Nucl. Mater.* **2006**, *359*, 220–226.
- [22] C. Anghel, Q. Dong, *J. Mater. Sci.* **2007**, *42*, 3440–3453.
- [23] Y. Xu, T. Åkermark, V. Gyollai, D. Zou, L. Eriksson, L. Duan, R. Zhang, B. Åkermark, L. Sun, *Inorg. Chem.* **2009**, *48*, 2717–2719.
- [24] K. Y. Koltunov, G. K. Surya Prakash, G. Rasul, G. A. Olah, *Eur. J. Org. Chem.* **2006**, 4861–4866.

Received: August 17, 2009
Published online: January 14, 2010